PHYSICAL REVIEW A VOLUME 6, NUMBER 3 SEPTEMBER 1972

Detailed Study of the Stark Broadening of Balmer Lines in a High-Density Plasma

W. L. Wiese, D. E. Kelleher, and D. R. Paquette
National Bureau of Standards, Washington, D. C.
(Received 23 March 1972)

The Stark-broadened profiles of the Balmer lines H_α, H_β, H_γ, and H_δ have been measured in a high-current, wall-stabilized arc operated in hydrogen. Temperatures and electron densities have been determined with a plasma model assuming partial local thermodynamic equilibrium (LTE), after a detailed plasma analysis revealed small deviations from complete LTE. The temperatures have been determined from line-to-continuum intensity ratios using H_β and continuum points in the near uv, and the electron densities were derived from absolute intensity measurements. The investigations cover the range of electron densities between 1.5×10^{16} and 10^{17} cm^{-3} and temperatures between 0.9×10^4 and 1.4×10^4 K. Extensive comparisons with recent Stark-broadening theories and other experiments have been undertaken with the following principal results: The most pronounced differences between this experiment and theory occur in and near the line centers, where the measured profiles show systematically less structure than the calculations predict. Comparisons of the calculated and precisely measured ratios between the $\frac{1}{2}$, $\frac{1}{4}$, and $\frac{1}{8}$ widths within *each* line show that the recent theories are internally consistent within 6% for H_β and H_γ, whereas for H_α inconsistencies of order 25% occur. Similar inconsistencies, somewhat larger respectively, are found for the theoretical values of the half-width ratios between *different* Balmer lines. For the most important line H_β, the measured half-widths agree within 7% with the calculated values. The total experimental error in this comparison, which originates predominantly in the electron-density measurement, is estimated not to exceed 6%. Very reproducible asymmetries and red shifts are observed for H_β and H_γ. Somewhat smaller red shifts are also obtained for H_α. The shifts are approximately linear functions of the electron density. Comparisons with other experimental data show appreciable scatter between the various results. We estimate that for the most-often-studied line H_β the uncertainties in the theoretical Stark widths are of the order of (5–7)% for the range of our experiment.

I. INTRODUCTION

Within the last few years three advanced theories of the Stark broadening of hydrogen lines have been developed. Kepple and Griem[1] applied a refined version of an earlier developed generalized impact approximation to the hydrogen lines H_α, H_β, H_γ, and H_δ. Smith, Cooper, and Vidal[2] described in a series of papers a "unified theory" based on classical path methods, and Voslamber[3] developed independently a very similar unified treatment of hydrogen line broadening. Numerical material is now available for the first two approaches, so that an extensive experimental test of these theories appears to be very much in order. Such a test is even more desirable because many available experiments do not provide adequate comparisons for these refined theories. For instance, the experimental comparisons often represent only spot checks for a particular set of conditions or for one particular line or for the ratio of two lines. Furthermore, many experiments do not possess sufficient precision to reveal finer details in the line profiles such as asymmetries, intensity distribution in the wings, structure near the line centers, shifts, etc. Finally, a number of inconsistencies between different experiments exist which are sometimes outside the combined estimated error limits. (Quantitative details will be given later when we compare the present data to the earlier experimental material.)

It has been the objective of this work to provide an extensive and detailed comparison with the recent theoretical treatments, to further improve the experimental precision in the line shapes and to give increased attention to finer details of the line shapes, such as asymmetries, structure near the line centers, and shifts.

II. EXPERIMENTAL PART

A. Plasma Source

The ideal plasma for radiation studies should be homogeneous as well as stationary. Since this is not yet technologically feasible for high-density, moderate-temperature plasmas, one has to make a choice between two basically different light sources; namely, either a stationary but inhomogeneous plasma as represented by a stabilized arc or a homogeneous but nonstationary source as represented by a shock tube. Our laboratory has been in the fortunate position of having both types of sources available, so that we had that choice. We decided to use a wall-stabilized arc as the one meeting most closely the above-mentioned ideal conditions. First, the wall-stabilized arc is a stationary source, which permits long-time integration and leads to excellent signal-to-noise

ratios. Secondly, its inhomogeneity is essentially only a technical drawback. It may actually be used to great advantage if the radial symmetry is properly utilized in side-on observations to provide simultaneously data for an extended range of plasma parameters. In such observations the application of a mathematical inversion process, the Abel inversion, permits the subdivision of the observed integrated intensity data into specific data from small homogeneous concentric ring zones of constant temperatures and densities. Thus, the geometrical configuration of rotational symmetry leaves no ambiguity as far as boundary layers and inhomogeneous end zones are concerned and indeed allows to a very close approximation the reduction of the data to homogeneous layers. Furthermore, it permits simultaneous observations over an extended range of densities. The inconvenience of the mathematical inversion process has been minimized with the extensive use of automatic data-processing equipment and computer programming.

The type of wall-stabilized arc employed in this experiment has already demonstrated its value as a dependable, accurate plasma source in many quantitative measurements of transition probabilities, continuous absorption coefficients, and line shapes, among which are very accurate transition-probability determinations in emission, not attained by any other source (e. g., Ne, Ar[4,5]). Its basic construction has been illustrated many times.[6,7] The arc is run between two tungsten electrodes, set about 10 cm apart. The arc column is confined and stabilized in its position by a number of water-cooled copper disks with an inner bore of 3 mm. These disks are electrically separated from each other by insulator rings, to which the windows for the side-on observations are attached. The height of the copper disks is empirically dimensioned in such a way as to prevent arcing through neighboring disks. Flat windows are positioned at the insulators about 3 cm away from the arc column, and the rear window is set at a slight angle from the normal to prevent multiple reflections. Purified hydrogen gas flows slowly into the central part of the arc and argon into the electrode areas. (For the study of the H_α profile, the arc is run in an Ar: H mixture in the atomic ratio 95: 5 in order to reduce self-absorption effects to insignificance.) All flow rates are regulated separately by flowmeters and are quite small—of the order of 100 ml/min. The gases are introduced tangentially into the relatively large cavities created by the insulating rings between the copper disks, and produce no noticeable disturbance of the arc. Effects on arc stability or asymmetries of the arc are only observed at flow rates being factors of 10 or more higher. The arc has four exit ports near the electrodes in order to keep the pressure at exactly 1 atm. In order to prevent any accidental leakage of the ambient air into the arc, the whole arc source is enclosed in a transparent box which is kept in argon at atmospheric pressure.

The operation of a stabilized arc with hydrogen as compared to other gases presents two special technical problems. First, the field strength in the arc column is very high. One needs therefore rather thin discs to prevent arcing between neighboring disks. Secondly, to achieve positive wall stabilization, the arc channel must be quite narrow, and the cooling of the arc pieces must be very efficient to withstand the energy released from the high-density plasma.

The arc is operated from a direct-current power supply specially constructed for precise arc operations. A total voltage of 800 V and a current of 40 A were supplied to the arc circuit which also contains a ballast resistor. The power supply makes use of silicon-controlled rectifiers for the current regulation. The (effective) current ripple (360 cps) is kept to less than 0.3%. The current stability over several hours running time, after a warm-up of 20 min, is about 0.2%.

The arc source, operated in this manner, has produced a very stable and reproducible spectra. Within each individual run, absolute intensity recordings at a given wavelength could be typically reproduced within 2% over time intervals as large as 10 h. The arc has been also checked for its short-time stability. Oscillograph records taken with different time resolution for signals originating predominantly from the axis or from the edge of the arc show only random noise and the ripple from the power supply. For a time resolution of a tenth of a microsecond, the over-all noise of the signal is typically $\pm 5\%$ at the arc axis and $\pm 8\%$ at the edge. For the reproducibility from run to run, taken at the same current, we have found that the absolute intensity of H_β determined in 13 runs covering a span of more than a year is typically kept within about 2% (standard deviation of single value from the mean).

B. Spectrometric Instrumentation and Calculation Equipment

The spectroscopic setup of this experiment differs from others applied to line-broadening studies by the inclusion of a predisperser, so that the radiation passes through two spectrometers in series. A schematic diagram of the instrumentation is given in Fig. 1. A $\frac{1}{2}$-m Ebert monochromator serves as the predisperser, and a 2.25-m Ebert spectrometer as the main instrument. The arc column is viewed side on and is imaged with its axis parallel to the slit jaws on the entrance slit of the predisperser, using a concave mirror with

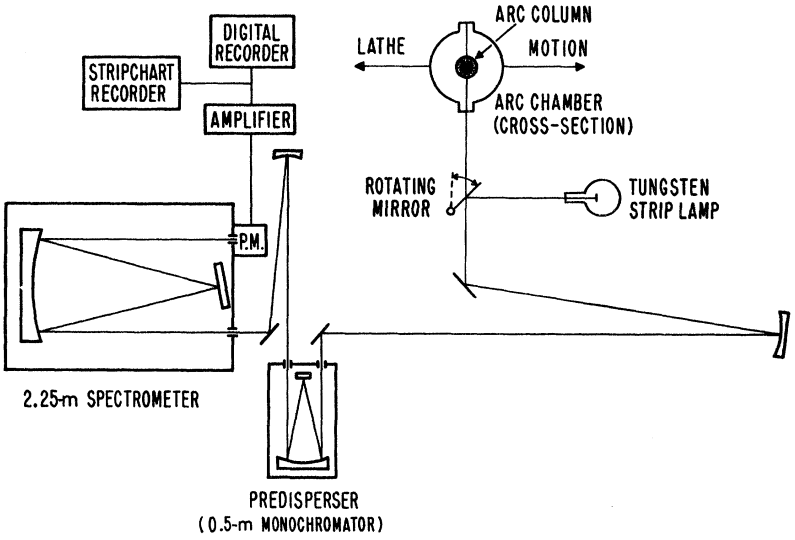

FIG. 1. Schematic diagram of the experimental setup.

a magnification ratio of about 2:1. The entrance slit of the predisperser is normally set at 50 μ. The exit slit of the predisperser is left wide open to admit a bandpass of about 40 Å to the entrance slit of the main instrument, which is opened to 1.5 mm. The exit slit of the main instrument is set at 50 μ for the Balmer lines and opened to 500 μ for the continuum measurements. The effective aperture of the optical system is kept to about $\frac{1}{65}$ to ensure spatial resolution of the plasma to the order of 50 μ. With this aperture, with the above mentioned slit widths, and with gratings of either 600 lines/mm or 1800 lines/mm in the case of H_α, a spectral resolution of about 0.3 Å for the Balmer lines H_β, H_γ, and H_δ and a resolution of 0.1 Å for H_α is obtained. These values are experimentally derived from He and Hg line profiles emitted by Geissler tubes. For the continuum measurements, we have chosen bandwidths from 1–2 Å. For the measurements in the visible, second-order radiation was eliminated by the use of suitable glass filters.

The intensities are put on an absolute radiometric scale by comparisons with a calibrated tungsten strip lamp using the setup shown in Fig. 1. To achieve the highest-possible precision in the calibration, the tungsten strip lamp is operated simultaneously with the arc source, and its radiance is recorded alternately with the arc by employing a rotating mirror as indicated in Fig. 1. In this way the calibration is immediately performed at each wavelength at which the arc radiation is measured. Since each experimental run has lasted for 8–10 h, we have used an uncalibrated strip lamp as the "working" lamp and preserved our primary standard, a very precisely calibrated lamp, for periodic comparisons with the "working" lamp. The calibrated standard lamp has been compared by the Optical Radiation Section at NBS with a blackbody at 21 wavelengths in the visible, near uv, and near ir. The working lamp was recalibrated every 50 h against the primary standard, which for this purpose was put in place of the arc. Small changes of order 1% have been found between the calibrations and have been taken into account. During the calibrations, the arc window was placed before the primary lamp at its usual position in the optical path in order to take its transmission loss into account. Of major importance has been the selection and reproduction of a well-defined area on the tungsten strip. Before each experiment we have therefore scanned slowly across the tungsten strip and produced a "map" in order to ascertain that the same preselected area is always used.

C. Data Collection and Processing

We have taken data in the following sequence: With the spectrometer and predisperser set at a preselected wavelength, we first record with a photomultiplier the zero signal for a period of 10 sec in 10 integration intervals of 1 sec each. Secondly, the radiative emission from the working strip lamp is recorded, with the rotating mirror M (Fig. 1) in the appropriate position. Again, a total integration time of 10 sec is used. Thirdly, the side-on arc image, from edge to edge, is scanned in a continuous motion across the spectrometer slit. The arc scanning is accomplished by advancing the arc on a lathe bed, utilizing the precision screw of the lathe. The length of the arc travel is determined by two adjustable electric limit switches mounted on the arc carriage. For a normal traverse scan of the arc, a total time of 1 min is used, subdivided into 60 integration intervals of 1-sec length. The direction of traverse is alternated, and the time of start is random within

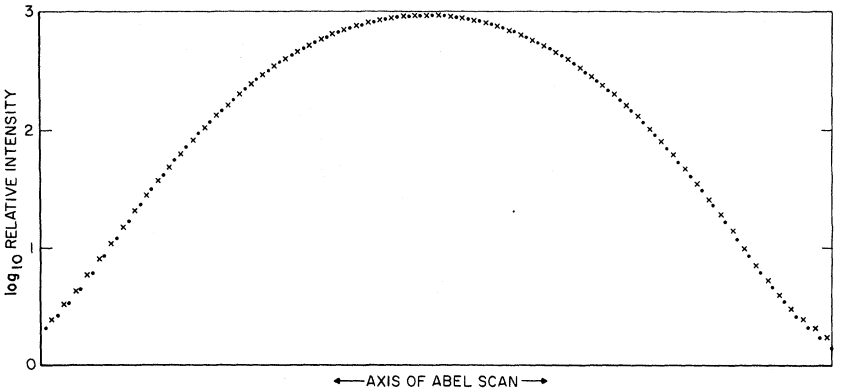

FIG. 2. Two superimposed sample traverses (points and crosses) across the arc. The direction of scan motion is reversed between the two runs to show the degree of rotational symmetry attained. Plotted are the digitized raw intensity data (integrated over small x increments) on a logarithmic scale vs the scan positions x.

1 sec after the closure of the limit switches.

The sequence of these three above-described recordings at any given wavelength takes up about 2 min after which the spectrometers are automatically advanced to the next selected wavelength. The automatic wavelength advance ensures that any hysteresis in the scanning drive mechanism produces consistently the same overshoot. The mechanical shutter, the rotating mirror, the start of the arc travel (in a back and forth motion), and the wavelength drive are all initiated electrically by switches assembled at the location of the experimenter. The limits of the arc travel on the lathe bed are approximately set before each experiment by observing the signal levels. Later on in the data processing, the signals at the arc edges are eliminated when they are below 0.5% of the peak signal at the arc center.

The signals are recorded with a digital data recorder. In addition, a 10-in. strip recorder is employed for on-the-spot monitoring of the signals. The digital data recorder is a special unit developed in our laboratories for the processing of arc intensity data[8] which are subjected to the Abel process. Its main components are a voltage-to-frequency converter, a counter, a shift register for the fast storage and readout of the counter and a paper-tape punch for recording. The unit has 0.001% linearity with a 5-digit capacity, mainly for dynamic range. The integration is preselected over any time interval up to 10 sec and is essentially continuous except for a 10-μsec transfer time of the data to the shift register. The continuous arc-scanning technique circumvents problems with mechanical hysteresis of the lathe. Due to the random start of the integration periods after opening of the limit switches, there are no biasing errors due to irregularities in the lathe motion or due to part-time integration. Finally, the signal-to-noise ratio is maximized by full-time integration.

The integrated arc signals, together with the standard lamp signals and the dark current readings, constitute the input to an Abel inversion program performed with a large electronic computer. Our program "preconditions" the raw data to better suit existing Abel methods, i.e., the data are numerically differentiated point by point using a fifth-order approximation to compensate for data integration, and are then corrected for the finite slit width and are finally truncated at signal levels of 0.5% of the maximum signal.

Our Abel inversion is based on a curve-fitting technique,[9,10] in which the data are integrated numerically to find the coefficients of orthogonal Legendre polynomials, and these coefficients are inserted into the solution to the Abel equation. The center of the Abel curve is the position along the scan axis corresponding to its center of gravity, and data are computed for about eight radial points of the arc and for each side. This Abel program, being probably one of the most refined in existence, nevertheless depends critically on the quality of the input data. The two principal requirements for these are large signal-to-noise ratios and rotational symmetry. We have therefore given careful attention to achieve these two things. Our signal integration technique to obtain large signal-to-noise ratios has been already described. The rotational symmetry of the arc column (which is also important for the precise determination of the arc depth) has been tested before and during each run by checking the degree of agreement between the data for the left- and right-hand side of arc traverses. Two examples representative of the achieved symmetry are given in Fig. 2. The intensities are given on a logarithmic scale, and significant deviations from symmetry are only noticed at levels less than 1% of the maximum.

It must furthermore be pointed out that we never depend on a single arc traverse, that is, on a single wavelength position, but rather on a large number of Abel-inverted scans (in alternating directions) to build up either a complete line profile or make measurements over a certain range of continuum wavelengths. Each wavelength position is calibrated independently; therefore, any errors which are

statistical in nature, like small asymmetries, will to a large part average out and become negligible in the final data analysis.

The Abel-inverted data are stored on computer cards and are thus conveniently available for the various plasma-analysis calculations.

D. Intensity and Line-Shape Measurements

In recent experimental line-broadening studies, much emphasis has been placed on the reliability of the plasma diagnostic method used for the independent determination of the electron density, but critical factors arising directly in the line shape and the intensity measurements have usually not received much attention. Since these may also contain significant error contributions, it seems appropriate to discuss the line-shape measurements proper in some detail. Likewise, the measurement of line and continuum intensities, on which ours as well as many other plasma analyses are based, has been rarely discussed in detail and shall be therefore reviewed here, too.

Our experimental line shapes are constructed from(side-on) intensity measurements at about 50–60 points over the range of each line. The following factors entering into measurement and analysis have been considered.

a. Possible nonlinearities in the photoelectric system. Precise tests of the linearity of a photoelectric recording system are rarely performed. We have checked our photoelectric system in the following way. We replace (see Fig. 1) the arc by a tungsten strip lamp, but leave the other lamp in its position. We furthermore substitute the rotating mirror by a fixed, half-silvered mirror (in the position indicated by the solid line in Fig. 1), and have ascertained that the beams from both strip lamps hit the identical area of the photocathode. The strip lamps are adjusted by current control to produce approximately equal intensity outputs. We then record digitally the intensities of each lamp and their combined signal. By comparing the sum of the two separate signals to the combined signal, the system may be thus precisely checked over a range of a factor of 2. The extension to the much-larger normal range of anode multiplier currents is then accomplished by varying the current of the strip lamps, allowing for sufficient overlap. Ten sets of measurements were taken at each current. Within our precision of 0.2% we find for the RCA 31000 photomultiplier used in this experiment a nonlinearity of 1.0% over the range from 10^{-9} to 10^{-6} A, with only 0.1% below 10^{-7} A. We find perfect linearity over this range for the 1P28 tube used in the H_α measurement. No multiplier fatigue is observed for these currents; this effect arises only for anode currents above 10^{-6} A.

b. Variations in spectral sensitivity. Variations in spectral sensitivity over the range of broad lines are often appreciable. For our spectrometer-detector system, we have found spectral sensitivity changes of 8% per 100 Å for the region H_β, 3% for H_γ, and 15% for H_α. They are taken into account by individual intensity calibrations at each measured wavelength.

c. Calibration of scanning motion of spectrometer. We have made an independent wavelength calibration by recording Fe I spectra obtained from a low-pressure electrodeless discharge. We used 145 Fe I lines in the range from 4000–5000 Å and plotted the differences between true wavelength and dial number versus wavelength. We found that these could be fitted to a straight line plus the first five terms in a Fourier series having the same periodicity as the screw which drives the grating of our 2.25-m spectrometer. The detected slight periodicity in the instrument causes an alternate compression and dilation of the wavelength scale by ±0.5 Å for every rotation of the screw, which is equal to 100 Å. Since this is of significance for the very broad Balmer lines, we have corrected for this by converting the monochromator dial numbers to the true wavelength scale.

d. Determination of the continuous background under the lines. The continuous background under the lines was determined in two steps. First, we measured the continuum intensities in two spectral ranges far away from the lines, in the regions between 5400 and 6000 Å and in the near uv from 2800–3600 Å. Contributions from the distant wings of the Lyman lines are negligible in the near-uv range, as we found from the application of theoretical asymptotic wing formulas. But, for the continuum range from 5400–6000 Å, the combined contributions of the Balmer-line wings have been calculated to be 2–4%, depending on the exact wavelength position, and have been subtracted.

In the second step, we have interpolated from these two measured spectral ranges to the region below the lines by applying the hydrogen continuum emission coefficients of Roberts and Voigt[11] in conjunction with our plasma diagnostic data. The near-uv and visible continuum regions have normally linked up within 3%, so that a very accurate interpolated background continuum under H_β and H_γ is indicated. The absolute intensity scale of the continuum is of course principally provided by the experiment itself, while Roberts's and Voigt's calculations furnish only the much-less-critical spectral distribution of the continuum. Typical numerical values for the background continuum, which we have computed for each measured wavelength, are for H_β about 1% of the maximum line intensity, and for H_γ about 5% of the maximum line intensity.

e. Impurities. Impurities in the plasma may

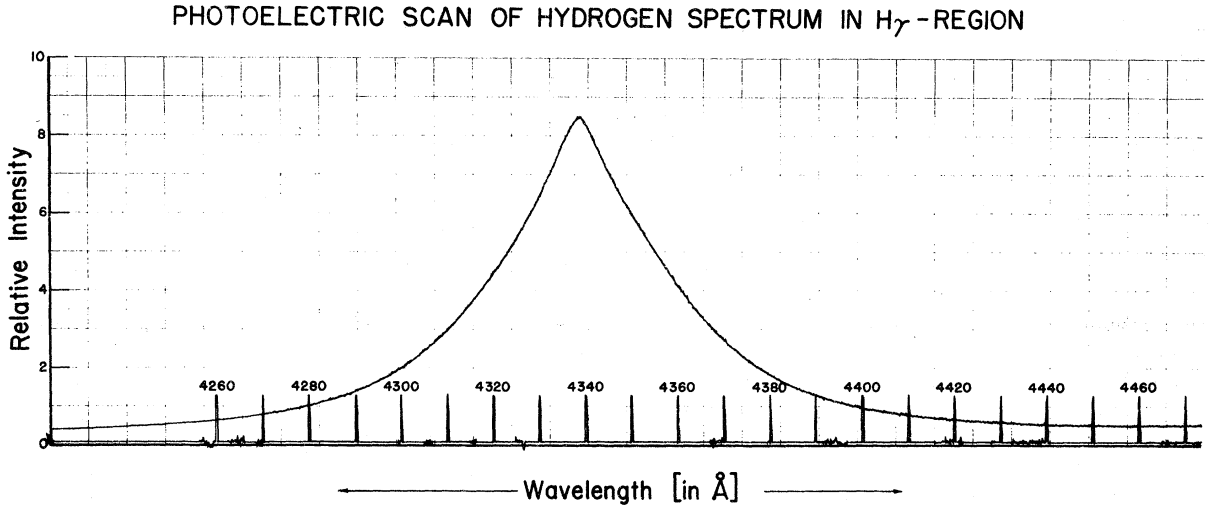

FIG. 3. Side-on scan with a strip chart recorder of the spectral region of H_γ to demonstrate the purity of the hydrogen spectrum and the excellent signal-to-noise ratio.

add weak-impurity line radiation within the range of the broad Balmer lines which might go undetected in the noise, but introduce a certain bias. We have made extensive scans of the hydrogen spectrum throughout the optical range and searched for impurity lines, but did not find any. There were not even traces of argon lines, which should be the strongest impurity due to our particular arc construction and enclosure. Figure 3 may serve as an example for the purity of the spectrum and the quality of the arc signals. The spectral region around H_γ is shown, but none of the prominent blue argon lines could be detected. On the basis of recently determined transition probabilities,[12] an upper limit for the argon impurity of 0.15% is obtained.

f. Self-absorption effects. The intensity $I(\lambda, l)$ emitted from a homogeneous plasma of length l in the wavelength interval $\lambda + \Delta\lambda$ in local thermodynamic equilibrium (LTE) is given by

$$I(\lambda, l)\,\Delta\lambda = B(\lambda, T)\,\Delta\lambda\,(1 - e^{-k(\lambda)l}), \tag{1}$$

where $B(\lambda, T)$ is the Planck function and $k(\lambda)$ is the (effective) absorption coefficient. For small optical depths, $\tau = k(\lambda)l \ll 1$, one obtains

$$I(\lambda, l) = B(\lambda, T)\,(\tau - \tfrac{1}{2}\tau^2 + \cdots) \tag{2}$$

or, with Kirchhoff's law $\epsilon(\lambda) = k(\lambda)B(\lambda, T)$ [where $\epsilon(\lambda)$ is the emission coefficient],

$$I(\lambda, l) = \epsilon(\lambda)l(1 - \tfrac{1}{2}\tau + \cdots). \tag{3}$$

If the measured intensities are to deviate by less than 1% from the true emission profile, the optical depth τ must be smaller than 0.02.

We have determined the optical depths by comparing the measured intensities of the line peaks $I(\lambda, l)_{max}$ with those of a blackbody at the arc temperature $B(\lambda, T)$. The ratio $I(\lambda, l)_{max}/B(\lambda, T)$ yields according to Eq. (1) the optical depth provided the plasma is spatially uniform. In our case, where the plasma is strongly inhomogeneous, we obtain an upper limit for H_β as well as H_α by using the intensity measured for the axial position multiplied by the effective depth of the arc. This depth is about 1.5 mm for the pure-hydrogen arc used for H_β, H_γ, and H_δ and about 2.0 mm for the argon-hydrogen mixture used for H_α. We have thus obtained upper limits: $\tau(H_\beta) < 0.0075$ and $\tau(H_\alpha) < 0.02$, and much smaller depths for H_γ and H_δ.

g. Other line-broadening mechanisms and instrumental broadening. For the temperature range of the arc the Doppler half-widths amount to about 0.5 Å or less for the studied Balmer lines, so that according to standard deconvolution procedures the contribution from Doppler broadening to the total measured half-width is negligible. The broadening due to other neutral hydrogen atoms (resonance and van der Waals interactions) has been recently calculated by Lortet and Roueff[13] and is for our conditions about an order of magnitude less than Doppler broadening.

The apparatus function has been determined by recording profiles of mercury and neon lines emitted from low-pressure discharges and from a He-Ne laser. We found that the approximately symmetrical apparatus function consists essentially of two parts. It has a narrow core of Gaussian shape with a half-width of 0.3 Å and very extended wings (which we could trace to distances of 2000 Å away from the line) of approximately Lorentzian shape. The changeover occurs when the intensity is about 10^{-3} of the maximum. This profile is quite typical for grating spectrometers, as shown for

example by Griffith,[14] and may be readily understood in terms of diffraction-grating theory, which predicts an asymptotic $\Delta\lambda^{-2}$ intensity distribution. Since the central part of the apparatus function is essentially Gaussian, with a half-width narrower than that due to Doppler broadening, the combined effect on the line profile is still negligible.

h. Scattered light. The extended wings of the apparatus function of the main instrument represent, under suitable conditions, a significant amount of scattered radiation.

For example, the continuum in the visible receives much more scattered light from the strong Balmer lines than it scatters away (the three strongest Balmer lines H_α, H_β, and H_γ emit under our operating conditions together about the same intensity as the total continuum in the visible). The continuum intensity is therefore raised by this additional radiation, as found by the introduction of a predisperser spectrometer, which reduces the intensity level of the continuum between H_α and H_β by almost 10%. Furthermore, the continuum radiated by the strip lamp is by orders of magnitude weaker in the near uv than in the visible , so that scattered light raises the near-uv lamp signals. These and other similar effects, like a net loss of intensity by the strong lines of order 1%, have been eliminated by using the predisperser. The application of a predisperser is especially important for continuum measurements, but has rarely been done before. Failure to include this was probably responsible for a significant part of our observed deviation between continuum and line intensities in our earlier hydrogen experiment.[15]

i. Line-wing contributions. We have included the contributions of the far wings to the total line intensity by applying the Kepple-Griem (KG) theoretical wing formula,[1] since it is impossible to determine this experimentally. We have used the KG wing formula[1,16] for wavelength distances beyond their tabulated values and find that this adds about 5% for H_γ and H_β to the line intensity.

j. Plasma length. For the determination of absolute line and continuum intensities, as well as for other plasma diagnostic techniques, the knowledge of the plasma length is required. The side-on scanning technique with the Abel inversion allows a particularly precise determination of this length, since both the lathe speed and the traverse time between the selected radial points are very precisely known.

III. PLASMA ANALYSIS

The determination of particle densities and temperatures is based on the measurement of several line and continuum intensities and includes the application of line-to-continuum ratios. We have proceeded with the plasma analysis in two ways.

A. Complete LTE Assumption

Since our plasma is purposely operated at high electron densities, we expect it to be strongly collision dominated. Estimates with available validity criteria[17,18] show that indeed, with one exception, complete LTE should be very well approximated in our source. The one exception is the insufficient fulfillment of a validity criterion for inhomogeneous plasmas. This criterion indicates that the critical length for the establishment of complete excitation and ionization equilibrium, which is the diffusion length of the ground-state atoms, is of the order of 500 μ.

Over such distances temperature changes of the order of a few percent or more occur so that no *local* temperatures and densities may be inferred from the intensity data. The tendency to smear out the local conditions is, however, not expected to produce major deviations from LTE (this is indeed confirmed by our second approach), so that the assumption of LTE should give a very useful first approximation for the analysis of the plasma.

For the high densities and the temperature range of our source from 9000 upwards to 14 000 K, the only important plasma species are the hydrogen atoms, protons, and electrons. All other species, like H^-, H_2, H_2^+, H_3, etc., are at least two orders of magnitude or much more below the aforementioned species and can be neglected in the composition calculations. Therefore, the LTE equilibrium and conservation equations are comprised simply of one ionization equilibrium equation (Saha equation) relating neutral hydrogen atoms (H), electrons (e^-), and protons (H^+); the equation of state (Dalton's law) and the condition of local electrical charge neutrality.[7] Debye corrections are applied to take the high-density effects into account.[19] Thus, a system of three equations is available for relating the four critical plasma parameters, i.e., the densities of the three above species plus the temperature. For the unique determination of these parameters, a fourth relation must be applied. We utilize here intensity measurements, since these quantities depend strongly on densities and temperature. We have overdetermined our plasma system by measuring the continuum intensities in the near uv and visible and the line intensities of H_β and H_γ. Since each of these intensities depends somewhat differently on the densities and temperature, as we shall see below, some checks can be made on the internal consistency of the assumed plasma model.

Expressed as a function of electron density (N_e), temperature (T), and wavelength (λ), the continuum intensity (in 10^{-7} W cm^{-3} sr^{-1}) is given by[11,15]:

$$I_\lambda^{\text{cont}} = \frac{32\pi^2}{3\sqrt{3}} \frac{e^6}{c^2(2\pi m)^{3/2}} \exp\left(-\frac{c_2}{\lambda T}\right) \frac{\Delta\lambda}{\lambda^2} \frac{N_e^2}{(kT)^{1/2}} \left\{ \frac{2E_H}{kT} \exp\left(-\frac{\Delta E_H}{kT}\right) \sum_{p_{\min}}^{15} \frac{g_{fb}}{p^3} \exp\left(\frac{E_H}{p^2 kT}\right) \right.$$

$$\left. + \bar{g}_{fb}\left[\exp\left(\frac{E_H}{16^2 kT}\right) - \exp\left(\frac{\Delta E_H}{kT}\right)\right] \exp\left(\frac{-\Delta E_H}{kT}\right) + g_{ff} \right\} + G(\lambda, T) N_e N_H \Delta\lambda + F(\lambda, T) N_{H^+} N_H \Delta\lambda \,. \quad (4)$$

The contribution of the H continuum is represented by the first term (to the end of the curly bracket) while the contributions of the H_2^+ and the H^- ions are given by the last two terms. N_H, N_{H^+}, and N_e are the number densities of hydrogen atoms (essentially the ground-state density), protons, and electrons, respectively; λ is the wavelength, T is the temperature, c_2 the second radiation constant, E_H the ionization potential of hydrogen, ΔE_H the lowering of the ionization potential,[19] p the principal quantum number, and g_{ff} and g_{fb} the Gaunt factors. For the visible region the summation over the free-bound continua was carried out from $p_{\min} = 3$ (Paschen continuum) to $p = 15$ (first term in the curly brackets), and for the near uv below 3650 Å the Balmer continuum $p_{\min} = 2$ is added. All free-bound transitions ending in higher p, which contribute only a very small fraction of the intensity, were approximately taken into account by replacing the sum with an integral (second term in the curly brackets). The upper limit for p is given by the last energy level below $E_H - \Delta E_H$. The third term in the bracket represents the contribution from the free-free continuum. The free-bound parts contain a factor $e^{-\Delta E_H/kT}$ which accounts for the lowering of the ionization potential. This factor does not apply to the free-free part, however. The quantities $G(\lambda, T)$ and $F(\lambda, T)$ are related to the absorption coefficients of H^- and H_2^+, respectively. For the experimental conditions, the H^- contribution becomes substantial at lower temperatures, especially in the visible spectrum. The H_2^+ contribution is at most a few percent. Numerical values for the continuum intensities were conveniently obtained from a computer program written by Roberts and Voigt for their extensive calculations of continuous hydrogen emission coefficients.[11]

The intensity of a hydrogen line is given for an optically thin homogeneous layer of unit length by

$$I_L = \int_{-\infty}^{\infty} I_\lambda d(\Delta\lambda) = (1/4\pi) hc (A/\lambda) N_p \,, \quad (5)$$

where the upper-state population is, in complete LTE, given by the Boltzmann factor

$$N_p = [2p^2/U(T)] N_H(T) e^{-E_p/kT} \,. \quad (6)$$

$2p^2$ is the statistical weight and E_p the excitation energy of the upper state p; A is the (exactly known) transition probability, and $U(T) = \sum 2p^2 e^{-E_p/kT}$ is the partition function.

For the determination of the total line intensities, the following contributing factors were considered. First, the underlying continuous background was subtracted according to the method described earlier. Second, contributions of the wings of other lines were also subtracted, employing the wing formula of Kepple and Griem[1] in conjunction with intensity data. Third, the area under the measured portion of the broadened lines was determined by a computer program using a Simpson's-rule integration, generalized to allow for unequal spacing. Fourth, the unmeasured portions of the line intensity in the wings were determined from the wing formula of Kepple and Griem[1,16] normalized so that the formula matched the data that lie farthest from the line center.

The relations for the continuum or line intensities, combined with the LTE equilibrium equations and the experimental intensity data, were then subjected to a Newton-Raphson iteration technique to find the nonlinear least-squares solution for T and N_e. The iteration was performed until the variations in T and N_e became less than one part in 10^5. For each experimental run, the plasma system was overdetermined by measuring two line intensities and two bands of continuum in the visible and uv. The electron densities resulting from these four separate intensity measurements are given in Table I (complete LTE assumption) and Fig. 4(a). In the table, the results of eight runs done under the same operating conditions are presented for a few selected radial positions. In the figure we show the over-all dependence on radial position for the electron densities, using the mean values from eight runs. These eight runs are highly independent: They were spread over the span of a year; before each run the arc was cleaned, reassembled, and realigned; the optical system was several times completely readjusted and the strip lamps were repeatedly recalibrated. Thus, the small, but very reproducible, differences which are observed between the "line" and "continuum" electron densities are significant. They are larger than the measurement errors and point to some systematic deviations from the assumed LTE model. The line-intensity data at the arc axis ($R = 0$) are too low compared to the continuum data, indicating an apparent underpopulation in the upper levels of these lines, while near the edge of the arc column ($R = 0.7$ mm) the situation is reversed.

A very plausible explanation for this behavior follows from the earlier stated estimate that an

TABLE I. Temperatures (in K) and electron densities (in 10^{16} cm^{-3}) derived from the spectroscopic data for three selected radial positions. The temperatures T are, for the complete LTE model, derived from the continuum data (visible and near uv); for the partial LTE model, they are derived from line-to-continuum ratios (electron temperature T_e). $N_e(H_\beta)$ denotes the electron density derived from the H_β intensity, etc.; uv refers to the near-uv continuum, vis to the visible continuum. N_e'(vis) is the electron density, in which the difference between gas and electron temperature is taken into account.

	Complete LTE assumption														
	Radial position $R=0.1$ mm					Radial position $R=0.5$ nm					Radial position $R=0.7$ mm				
	T	$N_e(H_\beta)$	$N_e(H_\gamma)$	N_e(uv)	N_e(vis)	T	$N_e(H_\beta)$	$N_e(H_\gamma)$	N_e(uv)	N_e(vis)	T	$N_e(H_\beta)$	$N_e(H_\gamma)$	N_e(uv)	N_e(vis)
Run No. 1	12950	8.41	8.44	8.77	8.84	11430	4.30	4.25	4.21	4.26	10210	2.21	2.08	1.86	1.89
2	12920	8.16	8.34	8.59	8.80	11380	4.01	4.08	4.06	4.10	10150	2.03	1.95	1.77	1.77
3	12920	8.22	···	8.58	8.74	11400	4.05	···	4.11	4.06	10080	2.07	···	1.67	1.76
4	12920	8.04	···	8.58	8.65	11370	3.98	···	4.02	4.03	10160	2.05	···	1.77	1.73
5	12920	7.97	···	8.58	8.77	11380	4.11	···	4.07	4.10	10140	2.17	···	1.76	1.81
6	12950	8.17	8.38	8.72	8.57	11320	4.02	4.10	3.93	3.89	10020	2.05	1.98	1.61	1.80
7	12950	8.30	8.52	8.73	8.80	11350	4.11	4.20	4.01	4.09	10060	2.11	2.04	1.65	1.85
8	12930	8.06	8.24	8.70	8.59	11360	4.02	4.07	4.05	4.13	10090	2.07	2.01	1.70	1.83
Mean values	12933	8.17	8.38	8.66	8.72	11374	4.08	4.14	4.06	4.08	10114	2.10	2.01	1.72	1.81
Std. dev. of mean (%)	0.04	0.62	0.56	0.33	0.42	0.03	0.89	0.87	0.71	0.89	0.07	1.1	1.1	1.7	1.0

	Partial LTE assumption														
	T_e	$N_e(H_\beta$,uv)	$N_e(H_\gamma)$	N_e'(vis)	N_e(vis)	T_e	$N_e(H_\beta$, uv)	$N_e(H_\gamma)$	N_e'(vis)	N_e(vis)	T_e	$N_e(H_\beta$,uv)	$N_e(H_\gamma)$	N_e'(vis)	N_e(vis)
Run No. 1	13740	9.05	9.00	8.84	8.88	11320	4.23	4.20	4.22	4.28	8900	1.82	1.77	1.80	1.87
2	13860	8.91	8.98	8.74	8.76	11340	4.08	4.13	4.06	4.14	8820	1.67	1.66	1.69	1.76
3	13650	8.81	···	8.73	8.76	11220	3.98	···	4.03	4.09	8650	1.65	···	1.67	1.75
4	14100	8.96	···	8.63	8.66	11610	4.09	···	4.01	4.07	8800	1.68	···	1.65	1.72
5	14330	9.06	···	8.61	8.63	11350	4.09	···	4.06	4.12	8560	1.70	···	1.71	1.79
6	14020	9.03	9.10	8.55	8.58	11220	3.96	4.04	3.85	3.92	8390	1.57	1.59	1.61	1.69
7	13910	9.07	9.16	8.78	8.82	11150	4.01	4.10	4.05	4.11	8360	1.61	1.63	1.73	1.81
8	14370	9.18	9.20	8.55	8.58	11580	4.11	4.14	4.11	4.17	8660	1.66	1.67	1.73	1.81
Mean values	13998	9.011	9.087	8.679	8.708	11349	4.070	4.122	4.049	4.112	8642	1.668	1.663	1.700	1.774
Std. dev. of mean (%)	0.68	0.46	0.39	0.44	0.54	0.53	0.75	0.53	0.90	0.68	0.82	1.5	1.4	1.4	1.1

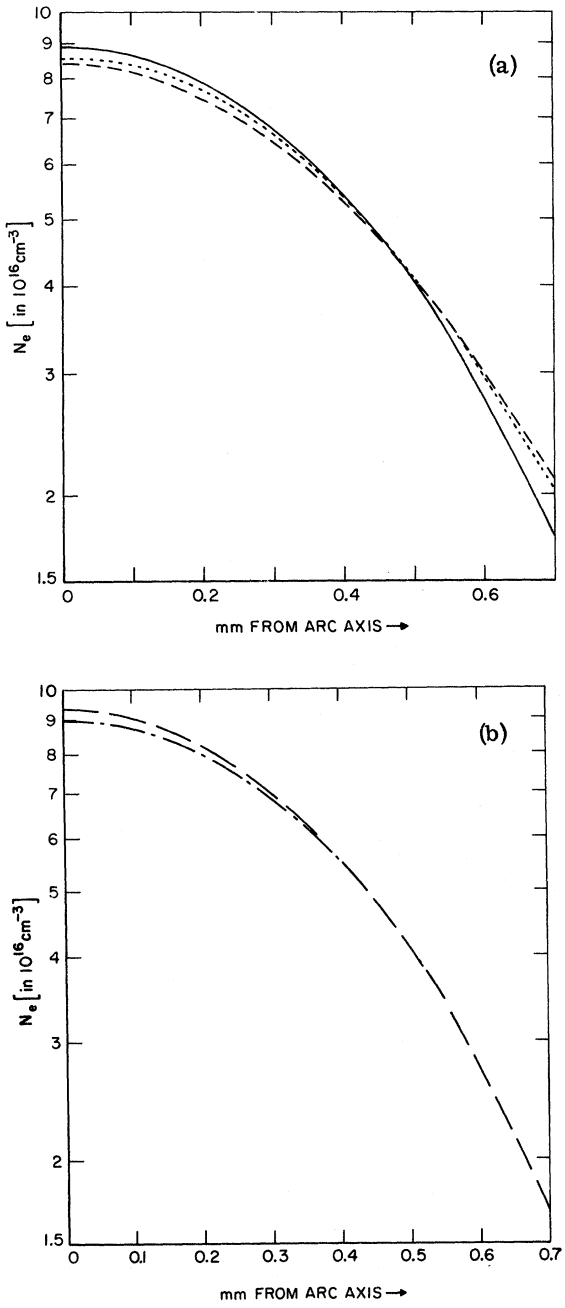

FIG. 4. (a) Dependence of electron densities on radial position. The curves are derived, under the assumption of complete LTE, from the following spectroscopic data: (solid line), absolute continuum intensity in the visible as well as near uv; (dashed line), absolute intensity of H_β; (dotted line), absolute intensity of H_γ. The data represent averages from eight runs, except for H_γ, where only five runs were used. (b) Dependence of electron densities on radial position under the assumption of partial LTE, based on the following spectroscopic data: Solid line, absolute intensity of H_β, or uv continuum, or H_γ; dot-dashed line, absolute intensity of the visible continuum. The data represent averages from eight runs, except for H_γ where only five runs were used.

LTE validity criterion for inhomogeneous plasmas is not well fulfilled. As noted above, the typical plasma length, over which the complete excitation and ionization equilibrium down to the ground state is established, has been calculated to be about 500 μ for out conditions. Over such a distance, as seen from Fig. 4(a), the temperature and electron density vary significantly. Therefore, the "local" temperatures (and densities) obtained under the assumption of complete LTE are to a certain degree averaged over this distance, and no true local values can be determined. The averaging effect is expected to be most strongly revealed in the experimental data which have the closest coupling to the atomic ground state, since it is the characteristic length for equilibration between ground state and lowest excited state which is so large. Indeed the data inferred from H_β, with its upper level in relatively close coupling to the ground state, appear to show the averaging effect more than H_γ and this line in turn more than the continuum. Because of the averaging effect, all these data are furthermore expected to be below the local electron temperature (T_e^{local}) at the arc axis, i.e.,

$$T_e^{\text{local}} > T_{\text{cont}} > T_{H_\gamma} > T_{H_\beta} .$$

The situation changes in a fundamental way for the cooler outer layers of the arc for two reasons. First, resonance radiation from the hotter axial region is strongly reabsorbed here and increases the excitation and ionization rates so that the equilibration for ground-state atoms becomes shorter. Second, diffusion currents become important due to the strong temperature and density gradients. According to the work of Uhlenbusch *et al.*[20] ambipolar diffusion of electrons and ions is especially significant. These mechanisms lead, in the cooler outer arc layers, apparently first to an equilibrium situation near $R = 0.5$ mm and then for larger radii to an overpopulation in the upper levels of the H_β and H_γ lines, which gives rise there to the relatively high line-intensity data of Table I (complete LTE assumption) and Fig. 4(a). Also, a similar overpopulation effect is expected for the continuum. The data show that the overpopulation of the H_β level is more pronounced than that for H_γ, and this in turn more than the continuum. Thus again the coupling to the ground state appears to be an important factor, and we expect

$$T_e^{\text{local}} < T_{\text{cont}} < T_{H_\gamma} < T_{H_\beta} .$$

B. Partial LTE Assumption

Since the ground-state hydrogen atoms are the critical quantity in the *complete* LTE model, we now modify our plasma analysis by abandoning the assumption of complete LTE down to the ground state. Instead we use in the following only the

much-less-critical assumption of *partial* LTE, i. e., equilibrium between the free electrons and the atoms in excited states down to the uppper level of $H_\beta(p=4)$. This assumption implies a common excitation and ionization temperature, the electron temperature T_e, for these states. The critical diffusion lengths for these excited states have been estimated to be of the order of 1 μ or less, [18] so that the inhomogeneity of the plasma is not problematical for the partial LTE description.

Our modified approach utilizes for the temperature determination the line-to-continuum intensity ratio, i. e., Eq. (4) divided by Eq. (5). This is nearly independent of N_e and N_H, if for the line intensity the upper-state population N_p of Eq. (5) is expressed differently from Eq. (6), in order to eliminate the connection to the ground state. For partial LTE this population is related to the electron density by a modified Saha equation, [18] which is for hydrogen

$$N_p = p^2 N_e^2 \left(\frac{2\pi m k T_e}{h^2}\right)^{-3/2} \exp\left(\frac{(E_H/p^2) - \Delta E_H}{kT}\right). \quad (7)$$

With this expression for N_p the line-to-continuum ratio is essentially only a function of the excitation temperature, except for the H^- and H_2^+ continuum contributions which are discussed below. (It is of interest to note that this ratio is practically independent of the high-density corrections.) For the experimental conditions, the optimum dependence of the line-to-continuum ratio on temperature is obtained by applying the line intensity of H_β and the continuum intensity in the ultraviolet. The use of the ultraviolet continuum intensity has the additional advantage that the contributions of H^- and H_2^+, which depend on the neutral hydrogen density, are rather small (about 4% for H^- and 1% for H_2^+ in the important central region of the arc) and may be taken care of by an iteration process which utilizes the equation of state in the form

$$P = (N_H + N_e) k T_g + N_e k T_e \quad (8)$$

for expressing the hydrogen density in terms of the electron density. P denotes the total plasma pressure (the prevailing atmospheric pressure) and T_g the heavy particle temperature. T_g is expected to be slightly below the electron temperature T_e, since the electrons receive primarily the energy from the applied electric field, but do not transfer this surplus energy completely to the heavy particles. (In the complete LTE model one assumes of course $T_e = T_g = T$.) Estimates of various degrees of refinement have been given for $(T_e - T_g)/T_g$, and recent detailed treatments for hydrogen arcs operating at conditions similar to ours[21] have resulted in numerical values ranging from about 1. 5% for the areas near the arc axis to 10% for the outer arc zones. In view of the considerable uncertainties in the transport cross sections required for these estimates, and the insignificance of this factor for the temperature determination, we have not undertaken analogous estimates and have applied this correction only to the electron density determined from the visible continuum as described below.

From the line-to-continuum ratios we have obtained the temperatures listed in Table I (partial LTE assumption). These are given for the same radial positions and runs as listed in Table I (complete LTE assumption). The scatter in the data is now much larger than before, since the ratio is a much weaker function of temperature than the absolute line and continuum intensities applied in the complete LTE model. At the arc axis the new "local" temperature is about 8% higher than those obtained before with the complete LTE assumption. This is consistent with the conjecture that T_e^{local} in the arc center should be somewhat higher than the "averaged LTE" temperatures. Away from the arc center, the "LTE" temperatures fall off slower than the new local electron temperatures, becoming equal at $R \approx 0.5$ mm and exceeding the local electron temperatures at larger radial positions, indicating there overpopulations of excited atomic states and free electrons which are probably due to reabsorption of resonance radiation from the hotter core and ambipolar diffusion. Uhlenbusch *et al.* [20] obtain qualitatively the same general tendencies in their work on He arcs.

With the local electron temperatures at hand, one may derive from the measured absolute line or continuum intensities "local" electron densities. These are given in Table I (partial LTE assumption) and Fig. 4(b). For the lines, Eqs. (5) and (7) have been directly applied. For the continuum, a complication again arises from the above-noted circumstance that the H^- and H_2^+ contributions in Eq. (1) contain the neutral-hydrogen density. These contributions are from three to five times larger for the visible than for near-uv continuum. They range from about 17% for the axial region of the arc to 65% for the outer radial zones. Since therefore uncertainties in the H^- and H_2^+ absorption coefficients and in the difference $T_e - T_g$ become significant for the visible continuum, especially at large radii, the electron density obtained from the visible continuum (N_e^{vis}) cannot be considered nearly as accurate as the other values. We have presented in Table I (partial LTE assumptions) these electron-density data without and with accounting for the difference between T_e and T_g. N_e^{vis} refers to the case where we assume $T_e - T_g = 0$, and $N_e'^{\text{vis}}$ refers to the data where we have applied the earlier-mentioned values for $(T_e - T_g)/T_g$ from the work of Steinberger. [21] In Fig. 4(b) we have included $N_e'^{\text{vis}}$ in addition to N_e (H_β, uv). It is seen from Table

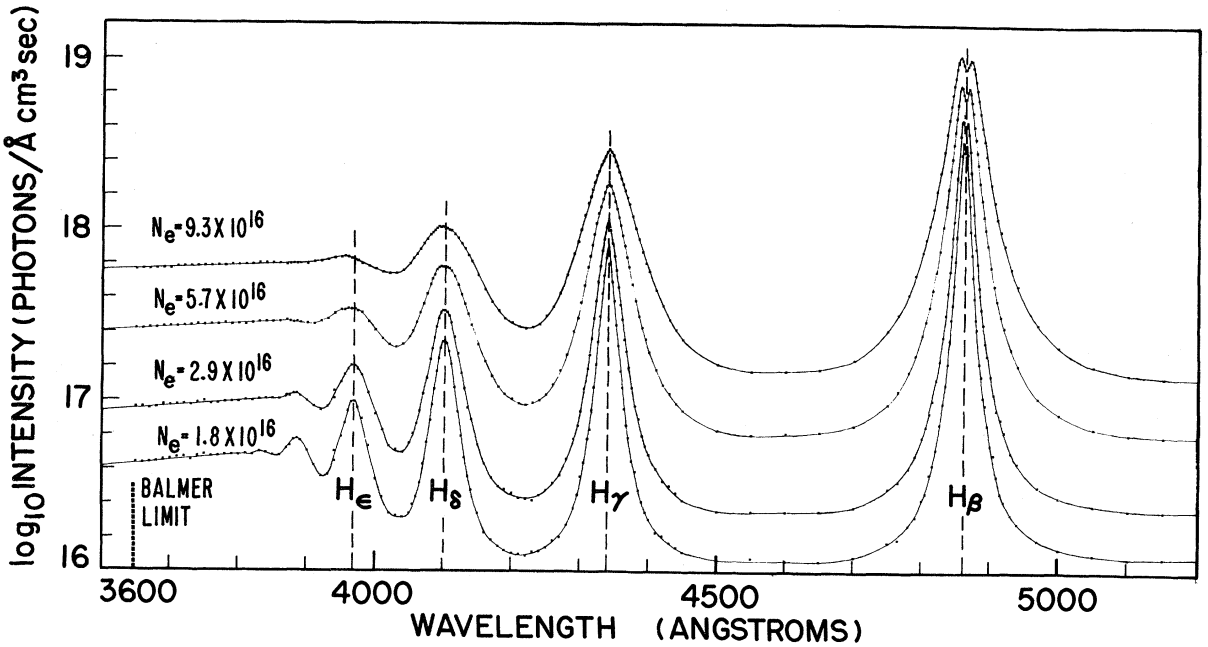

FIG. 5. Hydrogen spectrum from 3600–5200 Å. The four spectra represent four selected radial positions of the same run. The individual data points are connected by curves representing the best fit.

I (partial LTE assumption) and Fig. 4(b) that this correction essentially removes the differences between N_e^{vis} and the other electron-density data except for the central radial positions.

The internally consistent data from the partial LTE model (the less-accurate value for the electron density from the visible continuum intensity is not applied) will in the following be used for the analysis of the results and the comparison with the recent theoretical line-broadening data. It is of interest to note that the electron densities have changed by only about 3% from the complete LTE model for the important central region of the arc.

The line profile of H_α was measured in an argon-hydrogen mixture of the approximate atomic ratio 95 : 5. This became necessary since this line was strongly self-absorbed in a pure hydrogen plasma. We have measured the profiles of H_β and H_α and have used H_β as the comparison line. The Stark width of H_β and the correlation between the electron density and this width, as found in the pure-hydrogen arc, served for the determination of the electron density. The temperature (which has to be only approximately known) has been determined from the measured electron density under the assumption of the existence of complete LTE in the argon-hydrogen mixture.

IV. RESULTS AND COMPARISONS

A. Over-All Hydrogen Spectrum

Figure 5 shows, on a semilog scale, part of the spectral-intensity data from a single run. Four radial positions have been selected; the lines simply connect the data points. Not all measured continuum points are shown because of space limitations; the continuum data extend to 2800 Å toward shorter and to 6000 Å toward longer wavelengths. For each wavelength, the data points are interrelated through the Abel inversion process. But there is no connection horizontally between the individual data points; they are all individually calibrated with the procedure described earlier. A few selected points in the continuum, e. g., at 3600 Å, have been recorded repeatedly during the run in intervals of several hours. These data points fall so close together that they do not show up individually on the presented scale. An intensity range of about a factor of 2×10^3 is covered; nevertheless, no significant variation in the quality of the data is noticeable over the whole range.

Figure 5 shows instructively the variations in the spectrum as a function of electron density: the change in linewidth, the appearance of additional lines near the series limit at lower densities, the increasing filling-in of the continuum between the lines at higher electron densities, etc. It also shows the enormous amount of information obtained from side-on observations and the precision of our intensity measurements and of the Abel inversion technique.

B. Individual Line Profiles

In Figs. 6–9, we present the individual measured line profiles for the Balmer lines α, β, γ, and δ

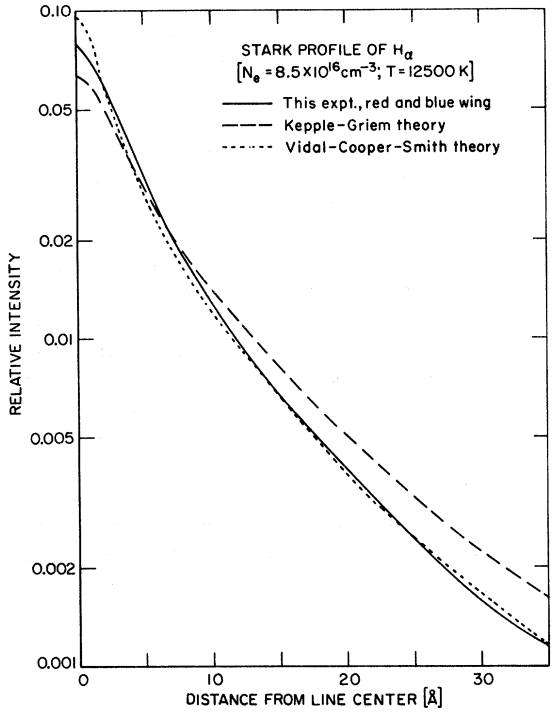

FIG. 6. Measured and calculated Stark profiles for H_α. Plotted is the normalized intensity on a semilog scale vs the wavelength distance from the line center. The experimental line center is defined as the average of the three points which bisect the $\frac{1}{2}$, $\frac{1}{4}$, and $\frac{1}{8}$ widths. It is for the conditions of this graph shifted by about 0.5 Å to the red.

and compare them with the recently calculated profiles of Kepple and Griem, [1] and Vidal, Cooper, and Smith. [22] All graphs give the relative intensity on a semilog scale versus the wavelength distance from the apparent line center. Total line intensities are all normalized to unity, i.e.,

$$\int_{-\infty}^{\infty} I(\lambda)\, d(\Delta\lambda) = 1 \,. \tag{9}$$

We have found the normalization of most KG profiles to be as much as 5% smaller than unity and have renormalized these. For the purpose of this comparison, we have suppressed measured shifts by taking the apparent "symmetry axis" of the shifted line (which we shall define later) as the point of origin ($\Delta\lambda = 0$) for the experimental profile. By folding the profiles about their apparent symmetry axis, a slightly different wavelength dependence of the red and blue wing, or, expressed

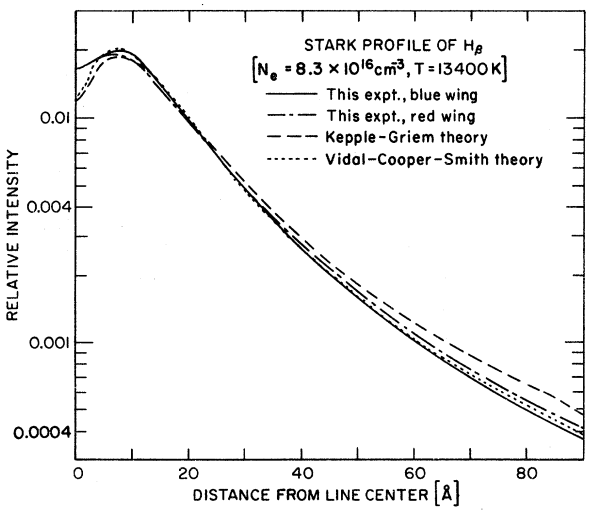

FIG. 7. Measured and calculated Stark profiles for H_β. As in Fig. 6, we plot the wavelength distance from the *shifted* line center. The red shift is about 0.6 Å.

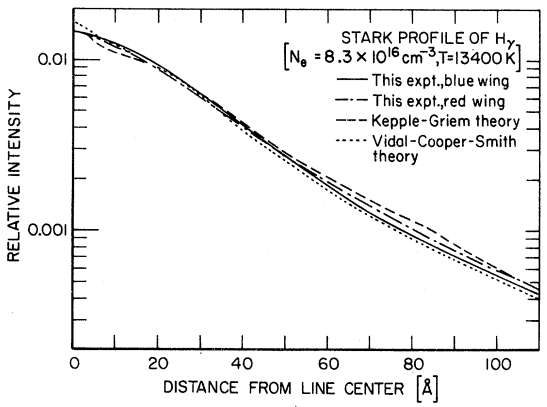

FIG. 8. Measured and calculated Stark profiles for H_γ. As in Fig. 6, we plot the wavelength distance from the *shifted* line center. The measured red shift is 0.7 Å.

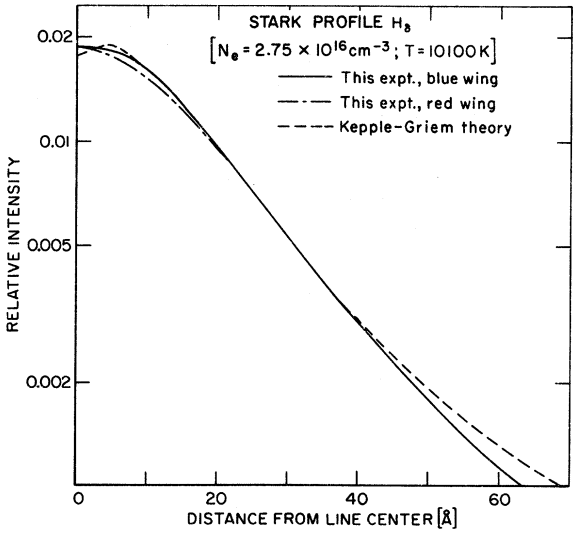

FIG. 9. Measured and calculated Stark profiles for H_δ. No shift is found for this line. The corrections for contributions of neighboring lines are considerable, especially for the blue wing.

differently, asymmetries in the lines, are most clearly revealed.

For the comparisons with the KG and Vidal-Cooper-Smith (VCS) calculations, it is convenient to discuss separately the line wings and the central parts of the lines and ignore the small asymmetries for the moment. (a) In the line wings, our measurements agree normally very well with the VCS calculations, while the KG profiles appear to be slightly too shallow, i.e., the slopes calculated by KG are slightly too small. This situation is most pronounced for the case of H_α (see Fig. 6). However, the slope of the KG asymptotic wing formula quickly approaches in the far wings that of the VCS calculations. This occurs in the graphs at the lower right, and it may be fairly well observed for H_β and H_γ. There is a corresponding discontinuity in the slopes at the point in the wings where the KG asymptotic formula takes over. (b) The major discrepancy between the calculations and the experiment occurs at the line centers. For the two measured lines with a pronounced central peak, H_α and H_γ, the VCS calculations yield peak intensities which are 20% and 10%, respectively, higher than the measured ones. The KG calculations deviate from the experiment for the case of H_α by 20% in the opposite direction, while for H_γ they agree very well with the measured peak intensity. For H_γ, both theories predict much more structure near the line center than is observed. For H_β, where all the Stark components are shifted, the main discrepancy is again at the line center. Both calculations yield central minima about 35% down from the peak intensities, in contrast to a measured dip of only about 15%. Since the line peaks are considerably displaced from the line center, the agreement there between the calculated and measured intensities is quite good. This favorable circumstance is probably largely responsible for the good accuracy and consistency of the theoretical fractional widths of H_β (which we shall discuss later). For H_δ, again a significant discrepancy occurs at the line center. The KG calculations (only these are available for H_δ) predict a small dip in the line center, while the experimental data show none.

Reasons for the discrepancies at the line centers are not well established. There are no apparent measurement problems: Doppler, van der Waals, and instrumental broadening as well as self-absorption effects are much too small to cause any noticeable modification to the measured Stark profiles, as we discussed earlier. The spatial resolution of the arc plasma is so high that it cannot cause any significant smearing of the experimental profiles, and the magnetic field produced by the arc current is much too small to cause any significant Zeeman splitting of the Stark components. Furthermore, similar discrepancies for the central dips in H_β and H_δ and for the center of H_γ have been also measured in other recent experiments.[23,24] Therefore, the most likely conclusion at this time is that the calculations produce too much structure in the line centers. Ion motion could conceivably reduce the structure, but it becomes negligible a few tenths of an angstrom from the line center.[25,26] The consideration of effects of inelastic collisions for the profile of H_β as calculated by Hill, Gerardo, and Kepple[23] raises the line center by about a fourth of the amount required for agreement with the experimental profile and lowers the peak by the same amount. This has the net effect that the discrepancy in the difference between the maximum and minimum is cut in half. However, the remainder of the profile is essentially unchanged, so that the lowered peak results in significantly reduced fractional widths, which increases the discrepancy with the experimental fractional widths. To obtain agreement with the experimental H_β profile, it is necessary to raise the line center out to the peaks without significantly affecting (except for normalization) the peak itself or the remainder of the profile. It seems therefore likely that there is some problem with the impact theory itself in the center of the lines. For example, several recent refinements by the inclusion of time ordering for L_α and L_β have raised the dip in those lines.[27,28]

Generally, there appears to be a trend toward better agreement at the line center with increasing upper-level quantum number of the line. This trend may be at least partly due to the gradually expanding validity of the quasistatic theory farther into the line center for the higher Balmer lines.

C. Linewidths

Kepple and Griem[1] have derived from their calculated profiles the reduced line widths α_n at $n=\frac{1}{2}$, $\frac{1}{4}$, and $\frac{1}{8}$ maximum intensity, which are *weak* functions of electron density and temperature. We have derived the same quantities also from the tabulated profiles of Vidal, Cooper, and Smith.[22] Experimental line widths $\Delta\lambda_n$ were determined by fitting a four-term polynomial through the six data points closest to the $\frac{1}{2}$, $\frac{1}{4}$, or $\frac{1}{8}$ widths. Width data were obtained from four runs for H_α, nine runs for H_β, and seven runs for H_γ. The reduced widths α_n are usually defined by

$$\alpha_n \equiv \Delta\lambda_n / F_0 = \Delta\lambda_n (2.61e)^{-1} N_e^{-2/3}, \tag{10}$$

where F_0 is the Holtsmark field strength. For a given experimental line profile, the electron density N_e is a constant; consequently, one should ideally obtain

$$(\Delta\lambda_n / \Delta\lambda_{n'})_{\text{meas}} = \alpha_n / \alpha_{n'}. \tag{11}$$

TABLE II. Comparisons of calculated and measured $\frac{1}{2}/\frac{1}{4}$- and $\frac{1}{2}/\frac{1}{8}$-width ratios (with standard deviations) within the Balmer lines. The comparison is specifically for the radial position $R = 0.2$ mm; however, the experimental and theoretical ratios change by less than 1% over the investigated range of conditions.

Line	No. of runs	$\Delta\lambda_{1/2}/\Delta\lambda_{1/4}$ or $\alpha_{1/2}/\alpha_{1/4}$ Expt.	KG	VCS	$\Delta\lambda_{1/2}/\Delta\lambda_{1/8}$ or $\alpha_{1/2}/\alpha_{1/8}$ Expt.	KG	VCS
H_α	4	0.534 ± 0.006	0.471	0.469	0.331 ± 0.003	0.281	0.262
H_β	14	0.659 ± 0.005	0.666	0.678	0.471 ± 0.004	0.472	0.486
H_γ	10	0.605 ± 0.005	0.587	0.597	0.428 ± 0.003	0.405	0.414

for the various widths within a line. The measured width ratios contain no significant systematic errors, and the standard deviations of the mean values are within 1%. Furthermore, the measured ratios are found to be constant within 1% for all radial positions of the arc, indicating that they are essentially independent of the electron density. Therefore, since any differences with the calculated ratios indicate internal inconsistencies in the calculated profiles, a comparison between measured and calculated ratios for the three different n's represents a sensitive check on the KG and VCS calculations. Such a comparison is presented in Table II. For H_β and H_γ the calculated and measured ratios agree within 6%; but for H_α large deviations occur, namely, 26% with the VCS width data and 18% with the KG width data, which appear to be mainly due to the earlier noted discrepancies at the line center.

The foregoing comparison was essentially independent of the electron density. It enters only through the choice of α which depends very weakly on it. In contrast, the following comparisons in Figs. 10–12 depend critically on N_e. These figures give a log-log plot of N_e versus either the measured (full) half-, quarter-, and eighth-widths or the corresponding widths from the KG and VCS calculations. The theoretical curves were generated by interpolating the α_n's with respect to the experimental temperatures corresponding to the independently determined electron densities; these α_n's were then converted to widths in angstroms. Thus, one may, for a given N_e, directly compare measured and calculated widths, or, for given width, compare the independent, spectroscopically derived, electron densities with those from the Stark-broadening theories. It is seen that for H_β the electron densities from the KG and VCS calculations are within 10% of the independently determined electron densities over our measured range of conditions. For H_γ the agreement with the KG calculations stays within 10%, while for the VCS data the agreement deteriorates to about 20%. For H_α, the agreement with both Stark-broadening theories is much poorer, which may be again readily traced to the discrepancies at the line center.

By fitting the measured widths to the average independently determined electron density, straight lines were obtained in the logarithmic presentations. Addition of higher-order terms did not improve the fit at all for H_β; the improvement in the

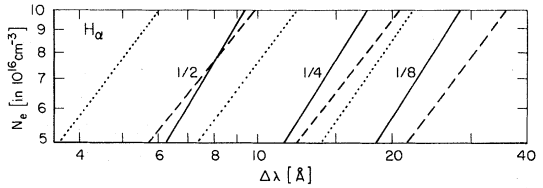

FIG. 10. Measured and calculated dependence of the $\frac{1}{2}$, $\frac{1}{4}$, and $\frac{1}{8}$ widths of H_α on the electron density. The H_α profiles were measured in a 95% argon, 5% (atomic) hydrogen plasma. The electron densities for the measured widths are the values obtained from the widths of H_β, using our measured relation between the widths of H_β and the electron density. The electron densities are for a range of temperatures from 1.1×10^4 to 1.3×10^4 K. The (very small) dependence of the theoretical width data on temperature is taken into account.

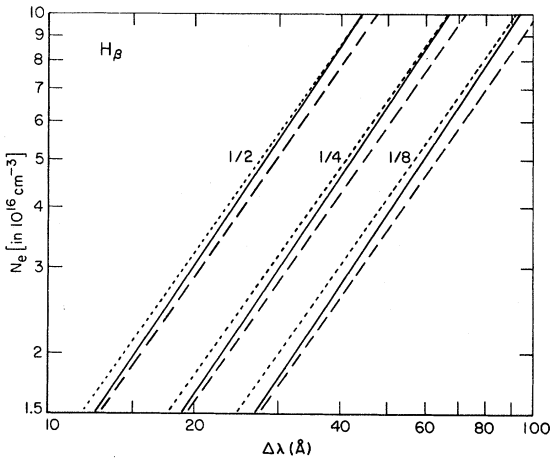

FIG. 11. Measured and calculated dependence of the $\frac{1}{2}$, $\frac{1}{4}$, and $\frac{1}{8}$ widths of the H_β on the electron density. The electron densities for the measured widths are the values obtained from uv continuum and line-intensity measurements discussed in the text. The electron densities are for a range of temperatures from 0.86×10^4 to 1.4×10^4 K. The (very small) dependence of the theoretical width data on temperature is taken into account.

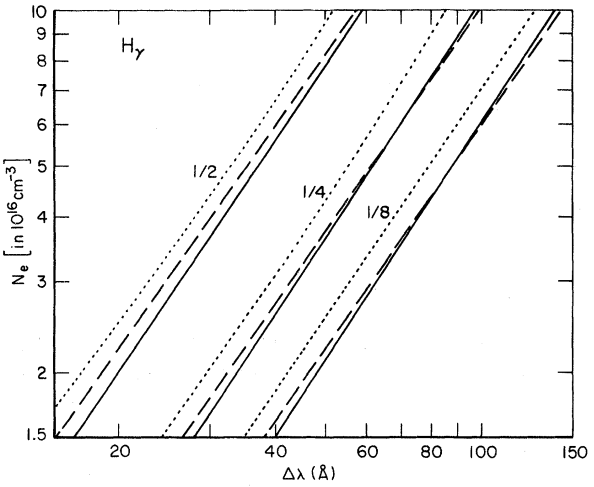

FIG. 12. Measured and calculated dependence of the $\frac{1}{2}$, $\frac{1}{4}$, and $\frac{1}{8}$ widths of H_γ on the electron density. (See also Fig. 11.)

standard deviation of the fit was less than 5% for H_α and H_γ. Thus, all experimental curves in Figs. 10–12, especially those for H_β, were measured to be linear over the indicated range of electron density. The slopes vary only slightly with different values of n. They are always slightly larger than the $\frac{3}{2}$ slope given by the Holtsmark theory (normally by 1–3%, for H_α up to 9%). The experimental slopes are also always slightly larger than the KG or VCS slopes, but less for H_γ and H_β than for H_α. We do not present the detailed numerical values for the slopes, since in the experiment, the temperatures as well as the electron densities vary. α_n is a weak function of both, which influences the slopes slightly and would make these data not generally useful for comparisons.

By comparing for a given electron density the corresponding widths for different lines, one may obtain from Figs. 10–12, for example, measured and calculated ratios of half-widths for H_β/H_γ or H_β/H_α. One observes then differences between the measured and calculated ratios, which are of the order of 5–15% for the H_β/H_γ ratio (for both calculations), but are much larger for the H_β/H_α ratio obtained with the VCS data. Since these width ratios depend only very weakly on the electron density and since the experimental width ratios are precisely measured, the differences indicate inconsistencies of the above quoted amounts between the various theoretical line profiles.

D. Asymmetries and Shifts

Asymmetries between the blue and red peaks of H_β have been observed many times before, but our measurements show for the first time that the asymmetries are a systematic, very reproducible feature extending all the way into the wings of H_β and H_γ, as seen in Figs. 6 and 7. (Within the precision of this experiment, no asymmetries are noticed for H_α. For H_δ, substantial corrections for the wing contributions of neighboring lines are necessary, which effectively prevent the observation of asymmetries for this line.) The asymmetries in H_β and H_γ always enhance the blue side over the red side near the line peak, but away from the line center a crossover occurs and the red wing is enhanced above the blue one. The calculations of KG and VCS, like all earlier calculations, do not take the asymmetries into account. But in a recent theory Sholin[29] singles out quadrupole interactions as the principal cause of the asymmetries and makes some quantitative estimates, which are in fair agreement with our observations (a preliminary account is given in Ref. 30).

Because of the shifts and asymmetries, the line centers have to be carefully defined. We have, for Figs. 6–9, defined the line center as the symmetry axis for the three points that bisect the $\frac{1}{2}$, $\frac{1}{4}$, and $\frac{1}{8}$ widths.

The magnitude of the shifts of the thus defined line centers is shown in a composite figure for H_α, H_β, and H_γ (Fig. 13). Each set of points represents a separate run. It appears that the shifts are directly proportional to the electron density. Further details for the shift of H_γ and their implications for white dwarf spectra have been already reported by us earlier.[31] A detailed discussion of the asymmetries and shifts and comparisons with Sholin's theory will be given elsewhere.

E. General Comparisons with Other Experiments

In Tables III and IV and Fig. 14 we have compiled some principal results from experimental Stark-broadening studies of the last ten years.[15,23,32–42] As we noted in the Introduction, many of the experiments have only the character of spot checks; namely, only one particular Balmer line has been studied or the ratio of the Stark widths between two Balmer lines has been measured, or the measurements are only performed at one particular value of electron density. We therefore have arranged separate comparisons for the various lines and linewidth ratios in Tables III and IV and Fig. 14.

It is no surprise that the experimental work has been concentrated on H_β: this line is located in a very accessible spectral range and it is fairly strong, but it is rather insensitive to self-absorption effects due to the lack of a central (unshifted) Stark component. All these factors have made this line a favorite for the study and for applications of Stark broadening. In Table III we could thus compile ten recent experimental results on H_β. The ratios of the electron densities derived from Stark-width measurements and from other independent spectroscopic methods are compared. A similar

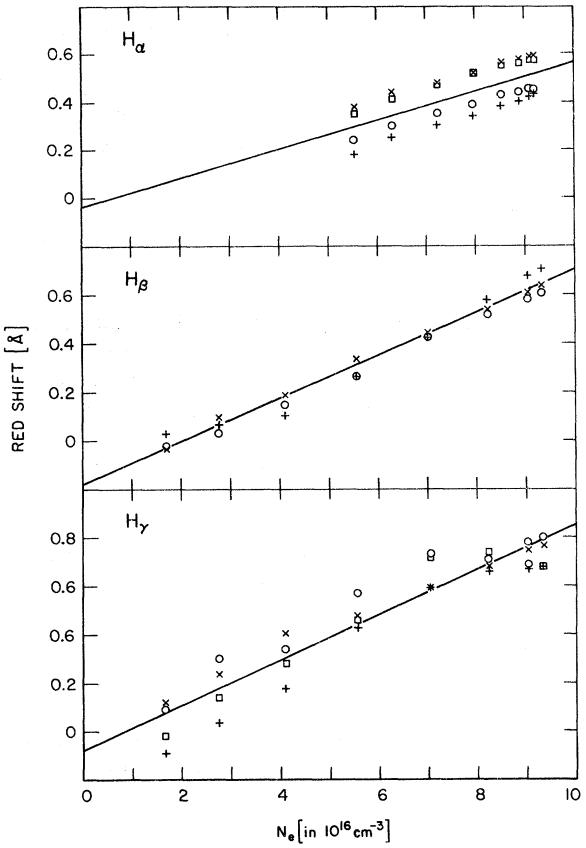

FIG. 13. Measured red shifts for H_α, H_β, and H_γ as a function of electron density. Symbols of the same kind indicate shifts measured for different radial positions of the same run.

comparison for H_β is made graphically in Fig. 14, where the (full) half-widths measured by various authors are plotted versus the electron densities obtained by different spectroscopic methods (see under diagnostic methods in Table III). In addition the Stark half-widths of KG are plotted versus electron density for the two temperatures of 10 000 and 20 000 K, which are approximately at both ends of the experimental range listed in Table III.

It may be observed from Table III that for H_β the measurements with pulsed sources yield generally slightly lower values for the electron density ratios than the stationary sources. On the other hand, no obvious correlations with the applied diagnostic techniques (Table III) can be noticed. (In order to obtain the comparisons with the KG and VCS Stark-broadening data, we have corrected the earlier experiments to account for the usually quite small changes from the then available Griem, Kolb, and Shen[43] data to the more recent theories.) Equivalently, Fig. 14 shows that a given measured width is usually correlated with a 5–10% higher electron density in a stationary source than in a pulsed

TABLE III. Comparison of recent experiments with the KG and the VCS theories. Given is the ratio between independently determined electron densities N_e^{diag} and the electron densities N_e^{KG} or N_e^{VCS}, obtained from half-width measurements and the theoretical Stark-width data of KG or VCS.

	Author (Ref.)	Plasma source	Diagnostic method for N_e	Temperature (10^3 K)	Range of electron density (10^{16} cm^{-3})	$\frac{N_e^{\text{diag}}}{N_e^{\text{KG}}}$	$\frac{N_e^{\text{diag}}}{N_e^{\text{VCS}}}$
H_α	Berg *et al.* (33)	*T* tube	Continuum	25	9.2	1.17	...
	Griffith *et al.* (32)	Free-burning arc	Fowler-Milne	10–20	2–18	0.78–0.89	...
	This experiment	Wall-stab. arc	Continuum	8.5–14	5–9	0.89–1.06	0.50
H_β	Berg *et al.* (33)	*T* tube	Continuum	14	8.0	1.01	0.92
	Hill *et al.* (23)	Pulsed source	Interferometry	21	1.5–7.5	1.01–1.03	0.92–0.95
	Konjevic *et al.* (34)	*T* tube	Interferometry	9.4–14.5	20–36	0.96–1.02	0.87–0.93
	McLean and Ramsden (35)	*T* tube	(a) Interferometry	17.6–20.9	20–27	(a) 1.01	0.95
			(b) Continuum			(b) 0.98	0.92
	Morris and Krey (36)	Pulsed arc	Fowler-Milne	16.7	20	1.05–1.08	0.98–1.01
	Shumaker and Popenoe (37)	Wall-stab. arc	Fowler-Milne	16.8	20	1.12	1.05
	Wende (38)	Wall-stab. arc	Line intensity	12	6.8	1.17	1.06
	Wiese *et al.* (1963) (15)	Wall-stab. arc	Continuum	10–12.5	3–7	1.06	0.96
	Foster (39)	Vortex arc	Line intensity	12		1.18	1.07
	This experiment	Wall-stab. arc	Continuum	8.5–14	1.6–9.3	1.04–1.11	9.92–1.01
H_γ	Berg *et al.* (33)	*T* tube	Continuum	14	9.4	1.08	1.02
	Hill *et al.* (23)	Pulsed source	Interferometry	21–26	1.5–7.0	1.03–1.04	0.90
	This experiment	Wall-stab. arc	Continuum	8.5–14	1.6–9.3	0.90–0.95	0.80–0.84
H_δ	Hill *et al.* (23)	Pulsed source	Interferometry	21	1.2–2.6	1.06–1.07	...
	This experiment	Wall-stab. arc	Continuum	8.5	1.6	0.97	...

source. A difference of this order is expected when the pulsed source is at a significantly higher temperature than the stationary source. This is, for example, the case between Hill *et al.* (21 000–26 000 K) and our experiment. In other cases, we have not found any obvious explanation for this difference, but we estimate that self-absorption should be a contributing factor for some pulsed sources. Self-absorption is more likely to occur in these sources because of the much larger plasma lengths l ($l = 20$–150 mm, while a typical *effective* hydrogen-arc diameter is 1.5 mm). Using the N_e, T, and l data given by the various authors, one can readily estimate the optical depth at the line peak by applying

$$\tau_{\text{peak}} = k(\lambda)_{\text{peak}}\, l = \frac{\epsilon(\lambda)_{\text{peak}}}{B(\lambda, T)} l = \frac{hc}{4\pi\lambda} \frac{A}{B(\lambda, T)} N_p S(\alpha)_{\text{peak}}\, l\,, \tag{12}$$

with N_p given by Eq. (7). We obtain for H_β the following τ's: McLean and Ramsden, $\tau = 0.12$, i.e., about 6% self-absorption at the H_β peak [see Eq. (3)]; Berg *et al.*, $\tau = 0.09$; Konjevic *et al.*,[44] $\tau = 0.22$–0.94; Hill *et al.*, $\tau = 0.03$–0.06. Only Hill *et al.* and McLean and Ramsden have corrected their profiles for self-absorption. [The McLean and Ramsden correction for the half-width (1%) seems to be rather small; we estimate twice as much.] It may be readily estimated that for H_β self-absorption effects in the other experiments make the measured half-wdiths appear too large by about $(\frac{1}{6}\tau)\times 100$ (%), which is part of the effect observed in Fig. 14.

The data for the other lines and linewidth ratios assembled in Tables III and IV show a fairly large amount of scatter. A few results appear to be definitely inconsistent with all others: The calculated H_α/H_β half-width ratio of Vidal, Cooper, and Smith reflects again their problem with the H_α line center; the calculated H_γ widths by Bacon and Edwards[46] at the higher electron density seem to be definitely too high; and the H_α results of Griffith *et al.*[32] produce 10–20% higher H_α/H_β ratios than those listed in Table IV.

Thus, the over-all situation is still not satisfac-

TABLE IV. Comparisons between recent experiments and Stark-broadening calculations. Presented are the experimental and theoretical ratios of the half-widths between various Balmer lines. The measurements are approximately at the indicated temperatures T and electron densities N_e.

Author (Ref.)	Method	Half-width ratios $\alpha^i_{1/2}/\alpha^j_{1/2}$ or $\Delta\lambda^i_{1/2}/\Delta\lambda^j_{1/2}$ $N_e = 10^{16}$ cm^{-3}	$N_e = 10^{17}$ cm^{-3}
	H_α/H_β ($i=\alpha$; $j=\beta$) for $T = 1\times10^4$ K		
Kepple and Griem (1)	Calc.	0.16	0.22
Vidal, Cooper and Smith (22)	Calc.	0.14	0.13
Bacon (45) (for H_α) and Kepple and Griem(1) (for H_β)	Calc.	•••	0.24
Birkeland *et al.* (40)	Stab.-arc expt.	•••	0.24
Bridges and Wiese (41)	Stab.-arc expt.	≈0.19	≈0.22
This experiment	Stab.-arc expt.	•••	0.21
	H_γ/H_β ($i=\gamma$; $j=\beta$) for $T = 1\times10^4$ K		
Kepple and Griem (1)	Calc.	1.18	1.19
Vidal, Cooper and Smith (22)	Calc.	1.13	1.15
Bacon and Edwards (46) (for H_γ) and Kepple and Griem (1) (for H_β)	Calc.	1.24	1.50
Berg *et al.* (33)	T-tube expt.	•••	1.21
Bengtson *et al.* (42)[a]	Shock-tube expt.	1.21	1.21
Wiese *et al.* (1963) (15)	Stab.-arc expt.	1.23	1.14
This experiment	Stab.-arc expt.	1.29	1.34
	H_γ/H_β ($i=\gamma$; $j=\beta$) for $T = 2\times10^4$ K		
Kepple and Griem (1)	Calc.	1.15	1.23
Vidal, Cooper, and Smith (22)	Calc.	1.17	•••
Bacon and Edwards (46) (for H_γ) and Kepple, and Griem (1) (for H_β)	Calc.	1.21	1.42
Hill, Gerardo, and Kepple (23)	Pulsed-source expt.	1.13	1.23
Bengtson *et al.* (42)	T-tube expt.	1.19	1.19

[a]The data of Bengtson *et al.* (Ref. 42) as presented in their Fig. 2 are separated into data obtained with a conventional shock tube at low temperatures ($T = 10\,000$–$12\,000$ K) and those obtained with a T tube at high temperature ($T = 22\,000$ K).

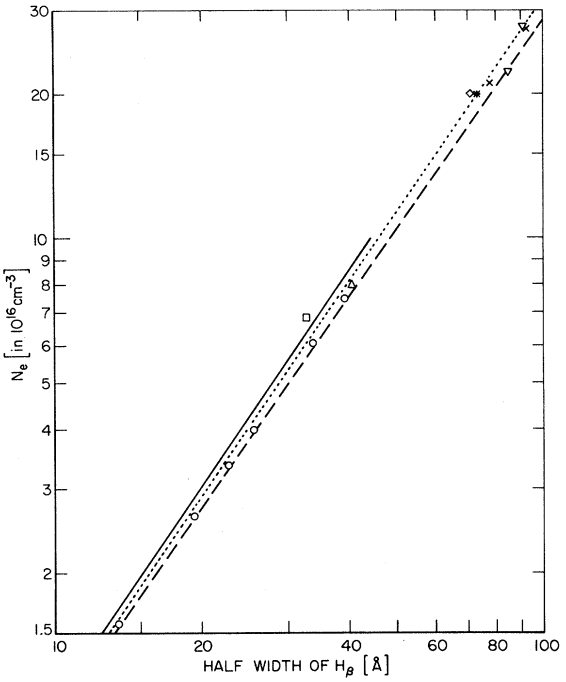

FIG. 14. Comparisons of experimental results for the relationship between half-width of H_β and (independently determined) electron density. Given are the results of the following authors: ○, Hill *et al.* (Ref. 23); △, Berg *et al.* (Ref. 33); ×, Konjevic *et al.* (Ref. 34); ▽, McLean and Ramsden (Ref. 35); ⁎, Morris and Krey (Ref. 36); ◇, Shumaker and Popenoe (Ref. 37); □, Wende (Ref. 38); (solid line), this experiment. Also included are the results of the Kepple and Griem (Ref. 1) calculations for 10 000 K (dotted line) and 20 000 K (dashed line).

tory. Definite reasons for the differences between the various experimental results are not readily found, since numerous significant factors enter into the measurements and calculations. In addition to the self-absorption effects discussed above, some other possible reasons are (a) slight deviations from complete LTE in inhomogeneous arc sources similar to the ones detected in this experiment (complete LTE has been always assumed). However, most other arc experiments have been done at somewhat different conditions, i. e., at higher electron densities and with argon as the principal carrier gas. Since argon exhibits typically a much wider arc column, deviations from LTE due to the inhomogeneity of the plasma are expected to be there much smaller. In our case the electron density in the arc center changed by only 3% from the complete to the partial LTE model, thus changes in the argon arcs should be insignificant. (b) Owing to the very short observation times in pulsed sources, the line profiles obtained with these sources are rather noisy, and often do not show finer details in the line shapes such as the well-known asymmetry between the two H_β peaks (see, e. g., Refs. 33 and 35). This may cause significant uncertainties in the linewidths, since the over-all line shape as well as the maximum intensity are not precisely determined. Furthermore, impurities, for example from electrode materials, should be much higher in these sources than in the better controllable arcs. Undetected weak-impurity lines could slightly distort the line shapes or raise the continuum (background) intensity levels. (c) For the pure-hydrogen plasmas as used in many experiments, the application of a predisperser for the measurement of absolute continuum intensities is quite important. Otherwise errors of the order of 5–10% in the continuum intensity may be encountered, i. e., the continuum produces a slightly high electron density, and the line-to-continuum ratio gives a temperature which is too high.

V. ERROR DISCUSSION

By using extensively automatic data-recording and -processing techniques, we could accumulate relatively large amounts of data with great ease. This large body of data makes possible a fairly detailed error analysis, which may be subdivided into three parts.

A. Statistical Measurement Errors

We have performed eight comprehensive runs under practically identical conditions (and several additional smaller runs), always using the same current setting, which has been controlled to 0. 1%. Before each run, however, the optical system was realigned, the arc reassembled, and slit widths set anew. The only other small difference between the runs is that they have been taken at slightly varying atmospheric pressures. By subjecting the plasma parameters to the standard statistical treatment, we have obtained the standard deviations for the mean values listed in Table V.

For the linewidths we obtained standard deviations of the mean values ranging from 0. 3–1%. These data are based on nine runs for H_β, seven runs for H_γ, and four runs for H_α.

B. Error Contributions from Input Data

A significant source of error in the input data originates from the absolute radiometric calibration. In addition to the standard deviations of the furnished radiances, given for the various wavelengths to be between 1% and $\frac{1}{2}$%, errors arise from uncertainties in the lamp current setting, and especially from our only approximate reproduction of the target area and solid angles specified in the calibration report. Furthermore, the strip lamp was found to be slightly polarized, but not the arc. A conservative estimate of the over-all relative

TABLE V. Standard deviations of the mean temperatures and electron densities obtained from eight runs with the partial LTE assumption.

Radial position (mm)	0.0	0.1	0.2	0.3	0.4	0.5	0.6	0.7
Mean local temperature (10^3 K)	14.10	14.00	13.67	13.18	12.35	11.35	10.07	8.64
Mean electron density (10^{16} cm^{-3})	9.32	9.04	8.22	7.03	5.55	4.08	2.74	1.67
Standard deviations of the mean values in %:								
Temperature	0.71	0.68	0.64	0.60	0.60	0.53	0.60	0.82
Electron density from H_δ	0.46	0.46	0.43	0.43	0.57	0.75	1.1	1.5
Electron density from H_γ	0.43	0.39	0.46	0.25	0.60	0.53	0.82	1.4
Electron density from uv continuum	0.46	0.46	0.43	0.43	0.57	0.75	1.06	1.5
Average electron density	0.46	0.43	0.43	0.43	0.57	0.71	0.96	1.4

error from these sources is 2%. The differences between the international practical temperature scale and the thermodynamic temperature scale are, however, fully taken into account by applying a correction factor containing the thermodynamic values of the natural constants.

Most atomic input data, including the Gaunt factors for the H continuum, are essentially exact quantities. But the H^- and H_2^+ absorption coefficients contain uncertainties estimated not to exceed 5%.[9] The H^- and H_2^+ contributions to the uv continuum, for temperatures near the arc axis, total about 6% and increase gradually to 16% for the outermost measured arc position. For the visible continuum on the other hand, the H^- and H_2^+ contributions amount to about 17% of the total continuum intensity in the arc center and increase to 65% in the outer radial zones. Thus, the over-all uncertainty in the uv continuum data ranges from only 0.3% for the axial position to 1% for the outermost radial position while the corresponding figures for the visible are 1–3.5%. This (as was noted before) has been one reason why only the uv continuum is used for the plasma analysis.

C. Uncertainties in Method of Analysis

A first contribution arises from the Abel inversion. The applied inversion technique has been therefore subjected to checks with analytical test functions which approximately resemble typical experimental input shapes. Superimposed on these curves has been random noise of the magnitude as encountered in the experiment. For these conditions the Abel inverted intensity data show only for the outer radial positions (typically $R > 0.5$ mm) deviations which are larger than 2% from the exact results. For the total line intensities as well as the average continuum intensities the possible deviations amount to much less since these intensities are built up from a large number of individual Abel data for the various wavelength positions. On the other hand, the linewidth measurements are somewhat more critical since many fewer points within a line are involved. Second, the line intensities may contain systematic errors from the use of approximate line-wing formulas. The intensity contained in the line wings is of the order of 5% of the total, so that a conservative estimate for the uncertainty it contributes to the total line intensity should be 2% or less. Third, the continuum intensities may be affected by scattered light as well as by contributions of far line wings. The effects of scattered light have been eliminated with the inclusion of the predisperser. We have calculated with the KG wing formula that the line wings produce in the measured continuum regions normally about 2% or less of the continuum intensity. Thus we estimate their contributions may be subtracted without significant error by using this wing formula. Fourth, the assumption of partial LTE is according to all criteria a very valid one and appears to be fully confirmed by the consistency of all our diagnostic data (in contrast to the complete LTE model). Fifth, for the lowering of the ionization potential in plasmas we have used the Debye correction,[19] which produces maximally a 7% change in the derived electron density (at the condition of the arc axis). While the Debye correction is now the generally accepted high-density correction, there is as yet no direct experimental confirmation. We thus find it impossible to assign error estimates on the last two points.

Using standard error analysis, we have obtained limits of error of ±3% for the temperature and of ±6% for the electron density. These numbers do not change significantly over the whole range of conditions; they are only slightly larger for the outermost radial position than for the axial region of the arc.

The ratios between the electron densities obtained (a) from the linewidth measurements and (b) from the intensity measurements have the same uncertainties as the electron densities, since the additional (independent) error in the linewidth determination is insignificant. The data for the ratios of widths within each line and between the different Balmer lines are only affected by the statis-

tical measurement errors, which are typically about 1%.

VI. SUMMARY

In conclusion, this experimental Stark-broadening study has yielded the following main results. (i) Systematic asymmetries and small shifts are observed for the first time in the Balmer lines, most clearly in H_β and H_γ. The asymmetries are systematic in the sense that for both lines near the line peak the blue side is stronger by a few percent than the red one, but then gradually a crossover occurs and the red side becomes a few percent stronger towards the line wings. The shifts are approximately linear functions of the electron density. Current theories do not give shifts or asymmetries. (ii) The most pronounced discrepancies between theoretical and experimental profiles occur near the line centers. The measurements show systematically less structure in the centers than the current line-broadening theories predict. For example, the measured dip for the center of H_β is only about one-third as deep as calculated by KG or VCS. (iii) According to Table II the calculations of KG and VCS are found to be—*within each line profile*—about equally consistent for H_β and H_γ where the $\frac{1}{2}$, $\frac{1}{4}$, and $\frac{1}{8}$ widths agree within about 6% with each other over the measured range of electron densities, while for H_α the inconsistencies between these widths are as high as 26%. (iv) We observe from Figs. 10–12 inconsistencies of the order of 5–15% between the measurements and the KG and VCS calculations when we compare the widths of H_β to H_γ. These inconsistencies become much larger for the VCS data involving H_α, and are apparently all attributable to their inaccurate description of the center of this line (see also Fig. 6). (v) All the above conclusions were obtained essentially without recourse to an independent electron-density measurement, assuming only that all linewidths are precisely measured in the same run. (vi) From independently determined electron densities, we find that for the most important line H_β the KG half-width data yield electron densities which differ by -4% (for the smallest N_e) to -10% (for the largest N_e) from our independently measured values over the investigated range. Correspondingly, the VCS data yield densities which differ by from $+9\%$ to -1% from the measured N_e's. (vii) Extensive comparisons with other recent measurements reveal appreciable scatter between the various experimental results. (viii) Our experiment shows that it is advantagous to use detailed line-profile measurements rather than half-width measurements for the determination of N_e by Stark broadening. This applies especially to H_α where a half-width measurement combined with the Vidal-Cooper-Smith data produces a value of N_e which is very different (and apparently wrong) from the detailed profile measurement and fitting, which is very satisfactory.

ACKNOWLEDGMENTS

We gratefully acknowledge the assistance of J. F. McClelland during the early phases of this work, and we would like to thank Dr. C. R. Vidal for permission to use his Stark-broadening tables before publication.

[1](a) P. Kepple and H. R. Griem, Phys. Rev. 173, 317 (1968); (b) P. Kepple, University of Maryland Report No. 831 (unpublished).

[2]E. W. Smith, J. Cooper, and C. R. Vidal, Phys. Rev. 185, 140 (1969); J. Quant. Spectry. Radiative Transfer 11, 263 (1971).

[3]D. Voslamber, Z. Naturforsch. 24a, 1458 (1969).

[4]J. B. Shumaker, Jr. and C. H. Popenoe, J. Opt. Soc. Am. 57, 8 (1967).

[5]J. M. Bridges and W. L. Wiese, Phys. Rev. 2, 285 (1970).

[6]H. Maecker and S. Steinberger, Z. Angew. Phys. 23, 456 (1968).

[7]W. L. Wiese, in *Methods of Experimental Physics*, edited by B. Bederson and W. L. Fite (Academic, New York, 1968), Vol. 7A, p. 307.

[8]D. R. Paquette and W. L. Wiese, Appl. Opt. 3, 291 (1964).

[9]M. P. Freeman and S. Katz, J. Opt. Soc. Am. 53, 1172 (1963).

[10]C. H. Popenoe and J. B. Shumaker, Jr., J. Res. Natl. Bur. Std. 69A, 495 (1965).

[11]J. R. Roberts and P. A. Voigt, J. Res. Natl. Bur. Std. 75A, 291 (1971).

[12]W. L. Wiese, M. W. Smith, and B. M. Miles, *Atomic Transition Probabilities*, Natl. Bur. Std. (U.S.) Monograph No. NSRDS-NBS 22 (U. S. GPO, Washington, D. C., 1969), Vol. II.

[13]M. C. Lortet and E. Roueff, Astron. Astrophys. 3, 462 (1969).

[14]R. F. Griffith, Monthly Notices Roy. Astron. Soc. 143, 319 (1969).

[15]W. L. Wiese, D. R. Paquette, and J. E. Solarski, Jr., Phys. Rev. 129, 1225 (1963).

[16]The KG wing formula given in Ref. 1(b), p. 16 contains an error. The factor e^{-y_1} that multiplies the terms $\frac{1}{5}$ and $\frac{4}{3}\,kT/E_H$ was inadvertently left out. This, together with the renormalization, made it necessary to reevaluate the values for the parameter d in the same formula.

[17]H. R. Griem, Phys. Rev. 131, 1170 (1963).

[18]H. W. Drawin, Z. Physik 228, 99 (1969).

[19]H. R. Griem, Phys. Rev. 128, 997 (1962).

[20]J. Uhlenbusch, E. Fischer, and J. Hackmann, Z. Physik 238, 404 (1970).

[21]S. Steinberger, Z. Physik 223, 1 (1969).

[22]C. R. Vidal, J. Cooper, and E. W. Smith (unpublished).

[23]R. A. Hill, J. B. Gerardo, and P. C. Kepple, Phys. Rev. A 3, 855 (1971).

[24]K. Behringer, Z. Physik 246, 333 (1971).

[25]V. I. Kogan, in *Plasma Physics and the Problem of Controlled Thermonuclear Reactions*, edited by M. S. Leontovich (Pergamon, New York, 1960), Vol. 4, p. 305.
[26]L. J. Roszman, Ph.D. thesis (University of Florida, 1971) (unpublished).
[27]M. E. Bacon, K. Y. Shen, and J. Cooper, Phys. Rev. 188, 50 (1969).
[28]H. Pfennig, J. Quant. Spectry. Radiative Transfer 12, 821 (1972).
[29]G. V. Sholin, Opt. Spectry. 26, 275 (1969).
[30]W. L. Wiese and D. E. Kelleher, *Proceedings of the Tenth International Conference on Phenomena in Ionized Gases* (Parsons, Oxford, 1971).
[31]W. L. Wiese and D. E. Kelleher, Astrophys. J. 166, L59 (1971).
[32]R. Griffith, L. Bober, and R. S. Tankin, Plasma Phys. 11, 529 (1969).
[33]H. F. Berg, A. W. Ali, R. Lincke, and H. R. Griem, Phys. Rev. 125, 199 (1962).
[34]N. Konjevic, L. Cirkovic, and J. Labat, Fizika 2, 121 (1970).
[35]E. A. McLean and S. A. Ramsden, Phys. Rev. 140, A1122 (1965).
[36]J. C. Morris and R. U. Krey, Phys. Rev. Letters 21, 1043 (1968).
[37]J. B. Shumaker, Jr. and C. H. Popenoe, Phys. Rev. Letters 21, 1046 (1968).
[38]B. Wende, Z. Naturforsch. 22a, 181 (1967).
[39]E. W. Foster, J. Phys. B 3, L145 (1970).
[40]J. W. Birkeland, S. P. Oss, and W. G. Braun, Phys. Rev. 178, 368 (1969).
[41]J. M. Bridges and W. L. Wiese, in *Proceedings of the Seventh International Conference on Ionization Phenomena in Gases* (Gradevinska Knyiga Beograd, Yugoslavia, 1966), Vol. III, p. 165.
[42]R. D. Bengtson, M. H. Miller, W. D. Davis, and J. R. Greig, Astrophys. J. 157, 957 (1969).
[43]H. R. Griem, A. C. Kolb, and K. Y. Shen, Astrophys. J. 135, 272 (1962).
[44]We have taken into account that an Ar-H_2 mixture in the ratio 9:1 has been used.
[45]M. E. Bacon, Phys. Rev. A 3, 825 (1971).
[46]M. E. Bacon and D. F. Edwards, J. Quant. Spectry. Radiative Transfer 9, 951 (1968).

PHYSICAL REVIEW A VOLUME 6, NUMBER 3 SEPTEMBER 1972

Molecular Dynamics of Hard Parallel Squares

C. Carlier and H. L. Frisch
State University of New York, Albany, New York 12203
(Received 29 February 1972)

Molecular dynamics of hard parallel squares subject to periodic boundary conditions appear to lead to a first-order phase transition with a van der Waals loop (at least for a system of 400 particles). The density change across the transition is small (about 2%). Results on the self-diffusion and velocity autocorrelation function $\rho(t)$ for 400 and 900 particles are also presented. $\rho(t)$ decays exponentially for short times, and at least in the intermediate fluid density, decays at t^{-1} for long times t. In the solidlike region anticorrelating effects predominate.

I. INTRODUCTION

Molecular dynamics (MD) of hard disks (HD) and spheres subject to periodic boundary conditions have been extensively studied for the past ten years by Alder and Wainwright. These dynamically simple systems are of great interest for providing insight into the adequacy of various approximate equations of state, the nature of phase transitions and the temporal behavior of the different autocorrelation functions of transport theory of real spherical molecules. The two dimensional system of hard parallel squares (HPS), subject to periodic boundary conditions, presents the same simplicity as the HD system with the interactions between particles arising solely from repulsive, impulsive forces. Moreover, the collisions between such HPS particles are even easier to compute. Our MD study of this system confirms a number of features observed in the elegant and pioneering work of Alder and Wainwright on the HD system and provides further computer experiments to test statistical mechanical theories.

A previous study of MD of the HPS system has shown qualitative evidence of a phase transition.[1] In Sec. II, we complete this study and show numerically at least that there is actually a first-order phase transition from the low-density fluid (fluidlike phase) to a more solidlike phase. Numerically we cannot demonstrate the presence or absence of long-range order in the latter but computer generated snapshots of the configuration of the particles suggest intuitively the name solidlike for that phase.

The pressure for solidlike and intermediate fluid densities are given and compared with the one obtained from theoretical expressions. A comparison with disks is presented at the end of Sec. II and in Sec. III where the interfacial tension between the two coexistent phases is calculated.

In Sec. IV, we present some results on the self-diffusion and velocity autocorrelation function $\rho(t)$